Journal of Physics: Conference Series **2894** (2024) 012024 doi:10.1088/1742-6596/2894/1/012024

Induced Photon Emission in Laguerre-Gauss Beams

Cesim K Dumlu[1], Yoshihide Nakamiya[1] and Kazuo A Tanaka[1,2]

[1] Extreme Light Infrastructure-Nuclear Physics (ELI-NP), 077125, Măgurele, Romania
[2] Institute of Laser Engineering, Osaka University, Yamada-oka 2-6, Suita, Osaka 565-0871 Japan

E-mail: cesim.dumlu@eli-np.ro

Abstract. We investigate stimulated photon emission in Laguerre-Gauss ($\mathrm{LG}_{\ell p}$) beams having arbitrary mode decomposition via Euler-Heisenberg Lagrangian. We look into the analytic structure of one-photon emission amplitude and identify its dominant and sub-dominant parts. In particular, we analyze three distinct nonlinear signatures associated with LG beams in which the orbital angular momentum (OAM) of the signal photon emerges as flipped, doubled or reduced with respect to OAM of incoming photons.

1. Introduction

The n-point photon amplitudes in QED encode coupling of electromagnetic fields via virtual quantum fluctuations and give rise to various nonlinear effects, akin to those encountered in the classical nonlinear optics [1]. These rich set of nonlinear phenomena (such as vacuum birefringence, stimulated/induced photon emission, photon splitting etc. see [2] for a recent review) are the tell-tale signatures for quantum fluctuations and have been analyzed in great detail over the years [3–19]. Now that the intense laser experiments are underway, there is a real chance to probe these phenomena in laboratory environment, which may provide access to QED structure coefficients, given by the leading order terms in Euler-Heisenberg lagrangian.

Here, we focus on induced photon emission, also known as the four-wave mixing, in which photons from the background field are absorbed and a signal photon is emitted at distinct harmonics. The induced photon emission at the microscopic level originates from the elastic scattering amplitude encoded by the QED box diagram. The cross section σ_{el} is exceedingly small therefore at first it might be natural to expect that the number of signal photons N would be negligibly small. On the other hand, several authors had realized that the number of scattering events in background field scale with the number of scattering centers, which in turn scale with the number of photons N_f inside the given focal volume, ultimately leading to an enhancement: $\sigma_{\mathrm{bg\ field}} \sim N_f \sigma_{\mathrm{el}}$. This observation was first made for a three-pulse collision geometry [20–22] yet similar enhancement was observed in two-pulse collision scenarios in later studies [13, 23], suggesting that the enhancement is in fact due to the nature of cubic coupling. Indeed, for the simple collision geometry where two Gaussian pulses collide head-on, It can be shown that signal photon number at the diffraction limit has the following scaling behavior:

$$N \sim \frac{4\alpha}{3}\frac{n^2}{90^2}\left(\frac{\lambda}{\lambda_c}\right)^4\left(\frac{E_0}{E_s}\right)^6 \tag{1}$$

Here n, λ_c and E_s respectively denote the number of cycles within the pulse, reduced Compton wavelength and the Schwinger critical field. Note that in the optical regime, $\lambda \sim 1\,\mu$m, the term $(\lambda/\lambda_c)^4$ brings in a volumetric enhancement considerably large enough that the signal photon yield can reach up to $\sim 10^3 - 10^4$, although the peak field strength E_0 could be well below the critical field strength. Therefore there is a real possibility to produce signal photons within thousands in future laser-laser collision experiments but the detection of signal photons is anticipated to be a challenging task. The main reason is that signal is predominantly produced along the external pulses and has the same frequency signature, making it difficult to distinguish from the background photons. For this reason the isolation of signal photons based on the properties such as polarization, frequency and angular spectrum becomes significant for their detection. In this respect, several works have focused on non-planar multi-pulse collision scenarios in which signal quanta can be emitted at higher harmonics along a direction isolated from the incoming beams [24, 25]. In a recent work [26], the authors have considered planar three-beam collision scenario where it was shown that orbital angular momentum(OAM) of the quanta inside external pulse can used as an additional filter to distinguish signal photons. Basic idea hinges on the fact that the outgoing signal quanta can be produced at different OAM signature than the background photons partaking in the reaction.

We extend this idea and explore the photon emission signatures resulting from the collision between Laguerre-Gauss ($\mathrm{LG}_{\ell p}$) beams of arbitrary mode decomposition. In Section II, we briefly revisit the theoretical aspects and discuss the dominant signatures belonging to photon emission amplitude. In Section III, we elaborate on the OAM signatures with the corresponding signal estimates. Final section contains our conclusions.

2. Theory

The total signal yield can be estimated by calculating the polarization summed transition amplitude to single photon state. For a head-on collision geometry between two linearly polarized beams, the signal yield can be given as($g_{\mu\nu} = +,-,-,-$) [27]:

$$N = \frac{16\alpha}{\pi^6}\frac{c^2}{90^2}\frac{1}{\lambda_c^4 E_s^6}\int |\vec{k}|^3\, d|\vec{k}|\sin\theta_k\, d\theta_k\, d\phi_k \left[\left(\sin^4\frac{\theta_k}{2}|\mathcal{S}(\vec{k})|^2 + \cos^4\frac{\theta_k}{2}|\bar{\mathcal{S}}(\vec{k})|^2\right) + \sin^2\frac{\theta_k}{2}\cos^2\frac{\theta_k}{2}\cos 2\phi_k\left(\mathcal{S}(\vec{k})^*\bar{\mathcal{S}}(\vec{k}) + \mathcal{S}(\vec{k})\bar{\mathcal{S}}^*(\vec{k})\right)\right] \tag{2}$$

Here (θ_k, ϕ_k) parametrize the photon emission angle with the momentum $(\hbar\omega/c, \hbar\vec{k})$. The Fourier amplitudes encode the cubic coupling of the fields,

$$\mathcal{S}(\vec{k}) = \int d^4x\, e^{ikx} E^2\bar{E}, \quad \bar{\mathcal{S}}(\vec{k}) = \int d^4x\, e^{ikx} E\bar{E}^2 \tag{3}$$

which respectively represent backward and forward emission amplitudes with respect to the optical axis chosen along $\hat{z}$. The external fields E and $\bar{E}$ are assumed to be transverse i.e $\vec{E}.\vec{H} = \vec{\bar{E}}.\vec{\bar{H}} = 0$ and $|\vec{E}| = c|\vec{B}|$, $|\vec{\bar{E}}| = c|\vec{\bar{B}}|$. They are modeled as real part of the pulsed $\mathrm{LG}_{\ell p}$ beam [28]:

$$E = \sum_{\ell p} E_0^{\ell p}\frac{w_0}{w(z)}\left(\frac{\sqrt{2}r}{w(z)}\right)^{|\ell|}\cos\left(\Omega(z/c-t) - \ell\phi + \phi_{\ell p} - (2p+|\ell|+1)\tan^{-1}\frac{z}{z_R} + \frac{z}{z_R}\frac{r^2}{w(z)^2}\right) \times e^{-\frac{r^2}{w(z)^2}} L_p^{|\ell|}\left(\frac{2r^2}{w(z)^2}\right) e^{-4(z/c-t)^2/\tau^2} \tag{4}$$

with waist size $w(z) = w_0\big(1 + z^2/z_R^2\big)^{1/2}$, central frequency Ω, Rayleigh length z_R and the pulse duration τ. The mode-dependent field strength can be inferred from the relation: $\varepsilon_0 c\big(E_0^{\ell p}\big)^2 \approx 8\sqrt{\frac{2}{\pi}}\frac{\mathcal{E}}{\pi w_0^2 \tau}\frac{p!}{(p+|\ell|)!}$, for the given pulse energy $\mathcal{E}$. Here, $L_p^{|\ell|}$ represents the associated Laguerre polynomial labeled by orbital angular momentum ℓ and the radial index p. Counter-propagating pulse $\bar{E}$ is defined via the replacement $z \to -z$ and has independent parameters which shall be denoted by the barred quantities: $E_{\bar{0}}^{\bar{\ell},\bar{p}}$, $\bar{z}_R$, $\bar{\Omega}$ and so on. Note that the Fourier amplitudes can be separated into positive negative frequency components ($s_i = \pm$) such that

$$\mathcal{S}(\vec{k}) = \frac{1}{8}\sum_{\substack{\ell_1,\ell_2,\bar{\ell}_3,\\ p_1,p_2,\bar{p}_3}}\sum_{s_1,\,s_2,\,s_3} S_{\{\ell,p\}}^{s_1 s_2 s_3}, \qquad \bar{\mathcal{S}}(\vec{k}) = \frac{1}{8}\sum_{\substack{\ell_1,\bar{\ell}_2,\bar{\ell}_3,\\ p_1,\bar{p}_2,\bar{p}_3}}\sum_{s_1,\,s_2,\,s_3} \bar{S}_{\{\ell,p\}}^{s_1 s_2 s_3} \tag{5}$$

where $\{\ell,\, p\}$ collectively denotes OAM and radial signatures of the signal. Upon performing the Fourier integrals, the signal amplitudes can be written as

$$\begin{aligned}
S_{\{\ell,p\}}^{s_1 s_2 s_3} =& E_0^{\ell_1,p_1} E_0^{\ell_2,p_2} E_{\bar{0}}^{\bar{\ell}_3,\bar{p}_3}\left(\frac{2\pi z_R^2 c\tau}{\Omega}\right)\left(\frac{\pi^{\frac{1}{2}}}{2\sqrt{\tau_{12}^2+2}} e^{-\frac{\tau^2}{16(\tau_{12}^2+2)}(|\vec{k}|c-(s_1+s_2+s_3\Omega_{21})\Omega)^2}\right)\\
&\times e^{i(s_1\ell_1+s_2\ell_2+s_3\bar{\ell}_3)\phi_k}\mathcal{F}_{\{\ell,p\}}^{s_1 s_2 s_3}\\
\bar{S}_{\{\ell,p\}}^{s_1 s_2 s_3} =& E_0^{\ell_1,p_1} E_{\bar{0}}^{\bar{\ell}_2,\bar{p}_2} E_{\bar{0}}^{\bar{\ell}_3,\bar{p}_3}\left(\frac{2\pi z_R^2 c\tau}{\Omega}\right)\left(\frac{\pi^{\frac{1}{2}}}{2\sqrt{2\tau_{12}^2+1}} e^{-\frac{\tau^2}{16(2\tau_{12}^2+1)}(|\vec{k}|c-(s_1+(s_2+s_3)\Omega_{21})\Omega)^2}\right)\\
&\times e^{i(s_1\ell_1+s_2\bar{\ell}_2+s_3\bar{\ell}_3)\phi_k}\bar{\mathcal{F}}_{\{\ell,p\}}^{s_1 s_2 s_3}
\end{aligned} \tag{6}$$

where we have defined $\tau_{12} = \tau/\bar{\tau}$ and also $\Omega_{21} = \bar{\Omega}/\Omega$. In the following we briefly mention few key points related to the structure of signal amplitudes given above. First, the terms $\mathcal{F}_{\{\ell,p\}}^{s_1 s_2 s_3}$ and $\bar{\mathcal{F}}_{\{\ell,p\}}^{s_1 s_2 s_3}$, whose explicit form can be found in [27], are dimensionless integrals along $\hat{z}$ direction and encode the angular spectrum of the scattered signal. The factor $2\pi z_R^2 c\tau/\Omega$ can be readily be identified as the four-volume factor. The remaining factors inside the parentheses encode the energy signature of the signal and in the limit: $\tau \to \infty$, they reduce to delta functions with the corresponding arguments. Remaining exponential terms represent the total OAM signature of the emitted photon. This signature depends on the energy signature, through the appearance of s_i, as well as the individual OAM of the photons partaking in the reaction. It is worth noting that not all the signatures equally contribute to the signal yield. First, it is evident that the negative energy signatures make no contribution to the signal amplitude because their support on $|\vec{k}| \in (0,\infty)$ virtually vanish. Further inspection of $\mathcal{F}_{\{\ell,p\}}^{s_1 s_2 s_3}$ and $\bar{\mathcal{F}}_{\{\ell,p\}}^{s_1 s_2 s_3}$ shows that among positive energy signatures, $\mathcal{F}_{\{\ell,p\}}^{++(-/+)}$ and $\bar{\mathcal{F}}_{\{\ell,p\}}^{(+/-)++}$ are exponentially damped because their phase oscillate rapidly. In addition, because of the symmetry associated with head-on collision geometry, the amplitudes have the exchange symmetry:

$$S_{\{\ell_1,\ell_2,\bar{\ell}_3,p_1,p_2,\bar{p}_3\}}^{s_1 s_2 s_3} = S_{\{\ell_2,\ell_1,\bar{\ell}_3,p_2,p_1,\bar{p}_3\}}^{s_2 s_1 s_3} \quad , \quad \bar{S}_{\{\ell_1,\bar{\ell}_2,\bar{\ell}_3,p_1,\bar{p}_2,\bar{p}_3\}}^{s_1 s_2 s_3} = \bar{S}_{\{\ell_1,\bar{\ell}_3,\bar{\ell}_2,p_1,\bar{p}_3,\bar{p}_2\}}^{s_1 s_3 s_2} \tag{7}$$

These observations ultimately lead to the conclusion that dominant signatures are given by the amplitudes $S_{\{\ell,p\}}^{+-+}$ and $\bar{S}_{\{\ell,p\}}^{+-+}$. In the following, we will use these amplitudes for the signal estimates under various collision scenarios.

3. Case Studies

Here, we summarize our results for the total signal yield and angular spectrum for scenarios in which the external beams will be chosen in various mode decompositions. For all cases we set

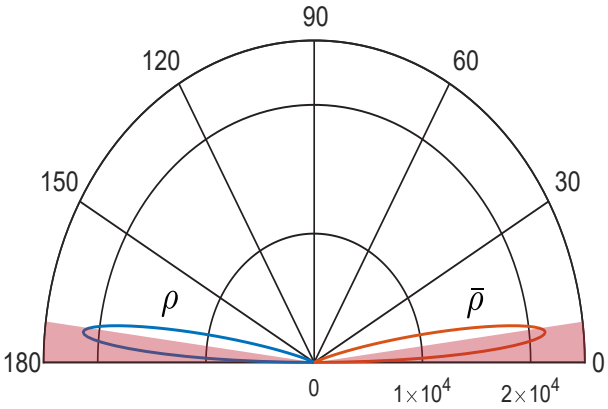

Figure 1. Angular spectrum of signal photon for backward (blue) and forward (orange) scattering for case 1. The divergence of the external beams are represented by the shaded (red) cones. Pulse parameters are given as: $\tilde{E}_0 = \tilde{E}_{\bar{0}} = 9.80648 \times 10^{-4}$, $w_0 = 2\,\mu$m, $\tau = 25\,$fs and $\lambda = 800\,$nm, yielding $N_{>\theta_d} = 3925$ (explained in the text). Note that we have dropped the subscripts $\{\ell, p\}$.

the radial index p and the carrier phase $\phi_{\ell p}$ to zero (henceforth, we drop p index and denote the amplitudes as $S^{+-+}_{\{\ell\}}$, $\bar{S}^{+-+}_{\{\ell\}}$). In addition, we will only be interested in forward and backward emission amplitudes; the interference term given in (2) is discarded. The reason for doing so is that $\mathcal{S}(\vec{k})$ and $\bar{\mathcal{S}}(\vec{k})$ are suppressed respectively in forward and backward direction, therefore their multiplicative contribution remains negligible.

To represent the angular distributions it is convenient to define a mode-dependent angular density functions, which depend on the dominant signatures only. By using (2), (5) and (6) we may write

$$\begin{aligned}
\rho_{\{\ell,p\}} &= \frac{2\alpha}{\pi^2}\frac{1}{90^2}\frac{c^4\tau^2}{\Omega^2}\left(\frac{z_R}{\lambda_c}\right)^4 \frac{\left(\tilde{E}_0^{\ell_1,p_1}\tilde{E}_0^{\ell_2,p_2}\tilde{E}_{\bar{0}}^{\bar{\ell}_3,\bar{p}_3}\right)^2}{\tau_{12}^2+2}\sin^4\frac{\theta_k}{2}\sin\theta_k \\
&\quad\times\int_0^\infty |\vec{k}|^3 e^{-\frac{\tau^2}{16(\tau_{12}^2+2)}(|\vec{k}|c-\Omega_{21}\Omega)^2}|\mathcal{F}^{+-+}_{\{\ell,p\}}|^2 d|\vec{k}| \\
\bar{\rho}_{\{\ell,p\}} &= \frac{2\alpha}{\pi^2}\frac{1}{90^2}\frac{c^4\tau^2}{\Omega^2}\left(\frac{z_R}{\lambda_c}\right)^4 \frac{\left(\tilde{E}_0^{\ell_1,p_1}\tilde{E}_{\bar{0}}^{\bar{\ell}_2,\bar{p}_2}\tilde{E}_{\bar{0}}^{\bar{\ell}_3,\bar{p}_3}\right)^2}{2\tau_{12}^2+1}\cos^4\frac{\theta_k}{2}\sin\theta_k \\
&\quad\times\int_0^\infty |\vec{k}|^3 e^{-\frac{\tau^2}{16(2\tau_{12}^2+1)}(|\vec{k}|c-\Omega)^2}|\bar{\mathcal{F}}^{+-+}_{\{\ell,p\}}|^2 d|\vec{k}|
\end{aligned} \tag{8}$$

where we have defined the normalized field strength $\tilde{E}_0 = E_0/E_s$. Note that above densities by definition include only the diagonal terms in $|\mathcal{S}(\vec{k})|^2$ and $|\bar{\mathcal{S}}(\vec{k})|^2$.

3.1. Pure Gaussian Collision

In the first scenario we consider both beams to be Gaussian and estimate the signal yield based on ELI-NP beam parameters [29]. For each pulse we take: $\mathcal{E} = 220$ J, $\lambda = 800$ nm and $\tau = 25$ fs and set the focal radius close to its diffraction limited value: $w_0 = 2\,\mu$m. The total signal photon yield is given by the amplitudes $S^{+-+} = \bar{S}^{+-+}$ where we have dropped $\{\ell, p\}$ indices. We find the signal yield as $N = 7727$. As seen in the angular spectrum (see Figure 1), a large amount

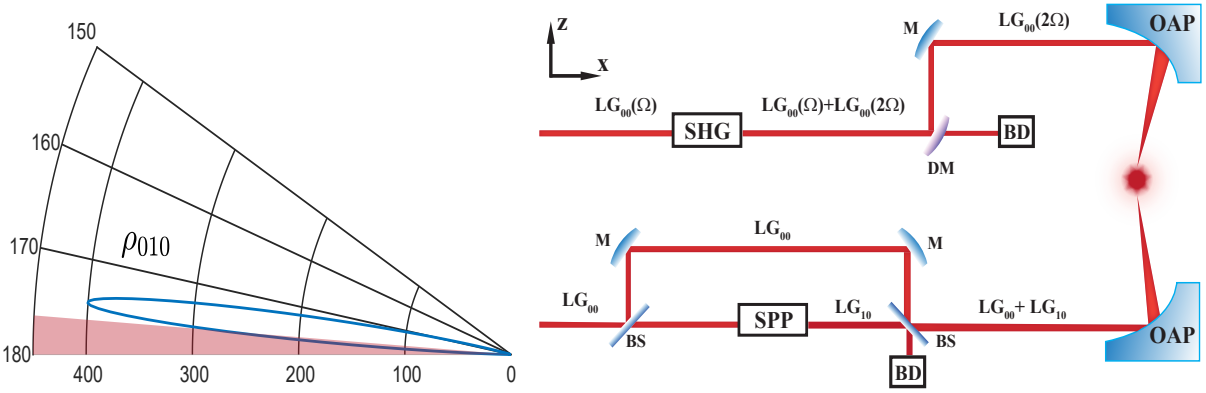

Figure 2. Left: Angular spectrum of signal photon for case 2. Pulse parameters are given as: $\tilde{E}_0^0 = 4.90324 \times 10^{-4}$, $\tilde{E}_0^1 = 4.33042 \times 10^{-4}$, $\tilde{E}_0^0 = 5.37123 \times 10^{-4}$, $w_0 = 2\,\mu$m, $\tau = 25$ fs and $\lambda = 800$ nm (counter-propagating pulse is frequency doubled), yielding $N^b_{010,>\theta_d} = 38$. Note that we have dropped the subscripts $\{p\}$.
Right: The schematics of the experimental setup probing the OAM flip. Lower arm of the 2×10 Petawatt laser arms at ELI-NP is split by 50:50 beam splitter (BS) The %50 of the source intensity is directed to Spiral Phase Plate (SPP), converting the incoming LG_{00} mode into LG_{10} mode with %78 conversion efficiency [32]. The output LG_{10} is combined with LG_{00} coming from the mirror (M) via 50:50 BS at a %50 loss in intensity and sent to the off-axis parabolic mirror (OAP). The upper arm is frequency doubled via second harmonic generation with %30 conversion efficiency. The resulting frequency doubled modes are picked by a dichroic mirror (DM) and sent to OAP for focusing. The remaining modes are directed to a beam dump (BD).

of these signal photons is emitted along the forward cones of the driving beams. The number of photons $N_{>\theta_d}$, outside the forward cones can simply be estimated by $N^f_{\{\ell,p\}>\theta_d} = \int_{\theta_d}^{\pi} \bar{\rho}_{\{\ell,p\}}\, d\theta_k$ for the forward emission, and by $N^b_{\{\ell,p\},>\theta_d} = \int_0^{\pi-\theta_d} \rho_{\{\ell,p\}}\, d\theta_k$ for the backward emission. The angle θ_d is the divergence half-angle: $\theta_d = M^2\lambda/\pi w_0$, where M is the beam quality factor [30]. We set M^2 to unity for (ideal)Gaussian beam. For higher order LG modes quality factor is given as: $M^2 = 2p + |\ell| + 1$ [31].

3.2. OAM Signatures

Here we will consider three particular cases, in which OAM of the signal photon respectively gets flipped, doubled and reduced with respect to the OAM of the incoming photons. First, to probe the flip signature, we consider the collision between two pulses, first of which is prepared in a mixture of LG_{00} and LG_{10} modes and the latter is prepared in the second harmonic LG_{00}. The schematics of the setup is displayed in Figure 2. We use the same set of parameters of the previous section for LG_{00} mode. For the second harmonic we set $\Omega_{21} = \bar{z}_R/z_R = 2$ and $\tau_{12} = 1$. Taking into account the efficiency factors (see Figure 2) and noting that the flip signature is given by the amplitude $S^{+-+}_{0\,1\,0}$, we find $N_{010} = 38$ signal photons emitted with $\ell = -1$, as a result of backscattering.

In order to estimate the yield for the OAM doubling signature we consider a scenario where both beams are given as a mixture of LG_{00} and LG_{10} modes. In view of the scenario outlined above, this case entails the split-recombination procedure on the both 10 PW arms. The relevant amplitudes in this case are given by $S^{+-+}_{1\,0\,1}$ and $\bar{S}^{+-+}_{1\,0\,1}$ Using previously chosen pulse parameters and the conversion efficiencies, we find $N_{101} = 15$ signal photons with $\ell = 2$ (see Figure 3).

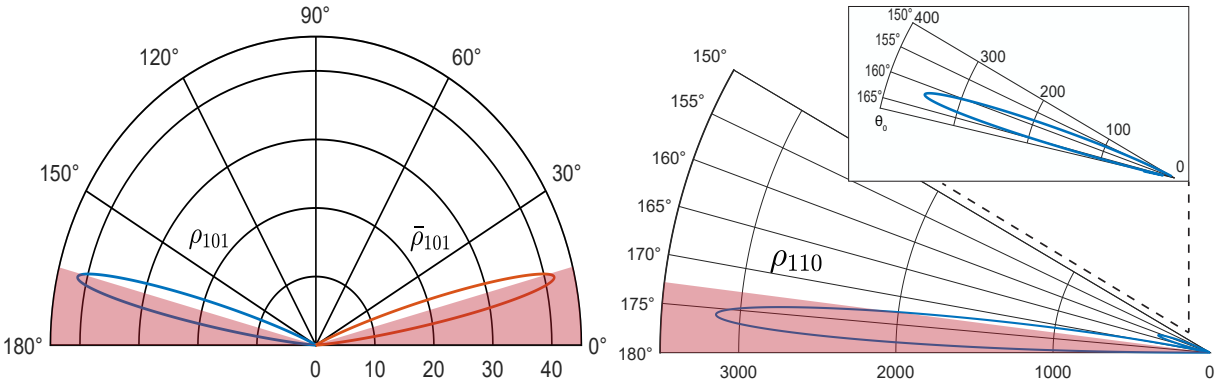

Figure 3. Left: angular spectrum of signal photon for backward and forward scattering for case 3. Pulse parameters are given as: $\tilde{E}_0^1 = \tilde{E}_{\bar{0}}^1 = 4.33042 \times 10^{-4}$, $\tilde{E}_0^0 = \tilde{E}_{\bar{0}}^0 = 4.90324 \times 10^{-4}$, $w_0 = 2\,\mu$m, $\tau = 25\,$fs and $\lambda = 800\,$nm, yielding $N_{>\theta_d} = 7$.
Right: angular spectrum of signal photon for backward scattering for case 4. Pulse parameters are given as: $\tilde{E}_0^1 = 8.66084 \times 10^{-4}$, $\tilde{E}_{\bar{0}}^0 = 9.80648 \times 10^{-4}$, $w_0 = 2\,\mu$m, $\tau = 25\,$fs and $\lambda = 800\,$nm, yielding $N^b_{110,>\theta_d} = 107$ and $N^b_{110,>\theta_0} = 46$

The final case involves collision between pure LG_{10} (propagating along $+\hat{z}$) and LG_{00} modes. This could in principle be achieved by sending one of the 10 PW arms directly to spiral phase plate whereas the beam coming from the other arm remains unaltered. The relevant amplitude in this case is $S_{1\,1\,0}^{+-+}$ whose distinguishing property is that the angular spectrum contains a non-trivial zero whose location is given by $\theta_0 = \pi - \arcsin\sqrt{6c/z_R\Omega}$ (see Figure 3). Around this minimum, the spectrum displays a multi-lob structure with two distinguished peaks for the signal. This structure signals a reduction in OAM (also referred as topological charge) meaning that the external photons with $\ell = 1$ scatter into a signal state with vanishing OAM. We find the total signal yield as $N_{110} = 401$.

4. Conclusions

In this study we have analyzed the analytic structure of the photon emission amplitudes, belonging to counter-propagating, pulse-shaped LG beams having arbitrary mode decomposition. We found that in head-on collision geometry the dominant contribution to the signal yield comes from $S_{\{\ell,p\}}^{+-+}$ and $\bar{S}_{\{\ell,p\}}^{+-+}$ when rapidly oscillating components are discarded. We have presented our estimates for the signatures, in which incoming photons can flip, double or reduce their OAM as a result of nonlinear coupling between the external fields. The yield for the OAM signatures are marginal due to the assumed losses yet, we should note, considering the overall scaling $N \sim \tilde{E}^6$, these figures can substantially be enhanced by increasing efficiencies and conversion factors.

Acknowledgments

We thank Felix Karbstein, Keita Seto and Takahisa Jitsuno for illuminating discussions. We acknowledge the support under the Contract No. PN 23 21 01 05 and ELI-NP Phase II project co-financed by the Romanian Government and the European Union through the European Regional Development Fund and the Competitiveness Operational Programme (Grant No. 1/07.07.2016, COP, ID 1334).

References

[1] Heisenberg W and Euler H 1936 *Z. Phys.* **98** 714
[2] Fedotov A, Ilderton A, Karbstein F, King F, Seipt D, Taya H and Torgrimsson G 2023 *Phys. Rep.* **1010** 1

[3] Di Piazza A, Hatsagortsyan K Z and Keitel C H 2006 *Phys. Rev. Lett.* **97** 083603
[4] Dinu V, Heinzl T, Ilderton A, Marklund M and Torgrimsson G 2014 *Phys. Rev. D* **89** 125003
[5] Karbstein F, Gies H, Reuter M and Zepf M 2015 *Phys. Rev. D* **92** 071301
[6] Bragin S, Meuren S, Keitel C H and Di Piazza A 2017 *Phys. Rev. Lett.* **119** 250403
[7] Ataman S 2018 *Phys. Rev. A* **97** 063811
[8] Bialynicka-Birula Z and Bialynicki-Birula I 1970 *Phys. Rev. D* **2** 2341
[9] Adler S L 1971 *Ann. Phys. (N.Y.)* **67** 599
[10] Baier V N, Milstein A I and Shaisultanov R Z 1987 *Phys. Lett. A* **120** 255
[11] Di Piazza A, Milstein A I and Keitel C H 2007 *Phys. Rev. A* **76** 032103
[12] Lundstrom E, Brodin G, Lundin J, Marklund M, Bingham R, Collier J, Mendonca J T and Norreys P 2006 *Phys. Rev. Lett.* **96** 083602
[13] J L, Marklund M, Lundstrom E, Brodin G, Collier J, Bingham R, Mendonca J T and Norreys P 2006 *Phys. Rev. A* **74** 043821
[14] King B, and Keitel C H 2012 *New J. Phys.* **14** 103002
[15] Gies H, Karbstein F and Kohlfurst C 2018 *Phys. Rev. D* **97** 036022
[16] Gies H, Karbstein F, Kohlfurst C and Seegert N 2018 *Phys. Rev. D* **97** 076022
[17] Blinne A, Gies H, Karbstein F, Kohlfurst C and Zepf M 2019 *Phys. Rev. D* **99** 016006
[18] Di Piazza A, Hatsagortsyan K Z and Keitel C H 2005 *Phys. Rev. D* **72** 085005
[19] Fedotov A M and Narozhny N B 2007 *Phys. Letts. A* **362** 1
[20] Mckenna J and Platzman P M 1963 *Phys. Rev.* **129** 2354
[21] Varfolomeev A A 1966 *Zh. Eksp. Teor. Fiz.* **50** 1024
[22] McDonald K T 1992 *AIP Conf. Proc* **279** 945
[23] Karbstein F and Shaisultanov R 2015 *Phys. Rev. D* **91** 113002
[24] King B, Hu H and Shen B 2018 *Phys. Rev. A* **98** 023817
[25] Gies H, Karbstein F and Klar L 2021 *Phys. Rev. D* **103** 076009
[26] Aboushelbaya R, Glize K, Savin A, Mayr M, Spiers B, Wang R, Collier J, Marklund M, Trines R, Bingham R and Norreys P 2019 *Phys. Rev. Lett.* **123** 113604
[27] Dumlu C K, Nakamiya Y and Tanaka K A 2022 *Phys. Rev. D* **106** 116001
[28] Plick W N and Krenn M 2015 *Phys. Rev. A* **92** 063841
[29] Radier C *et al.* 2022 *High Power Laser Science and Engineering* **10** E21
[30] Siegman A E 1993 *Proc. SPIE 1868, Laser Resonators and Coherent Optics: Modeling, Technology, and Applications* **1868** 2
[31] Saghafi S and Sheppard C 1998 *Opt. Commun.* **153** 207
[32] Sueda K, Miyaji G, Miyanaga N and Nakatsuka N 2004 *Opt. Express* **12** 3548